EUROPEAN ORGANIZATION FOR NUCLEAR RESEARCH
CERN - SL DIVISION

CERN-SL-99-038 BT

Transient quasi-static thermal stresses in a bar subject to transverse 2D-Gaussian heating and to lateral cooling

S. Péraire

Abstract

Many of the CERN secondary-particle production targets are plate shaped, and intercept a centred 'slow' extracted (order of ms) primary beam, which heats the material. This heat distribution can be modelled as Gaussian profiles in both the horizontal and vertical transverse planes. Modern techniques such as finite element methods provide fast and reliable analyses of the transient thermal and mechanical response of such a 'slow' process (no dynamic effects). However, it is of interest to compare these results with those obtained by simplified analytical calculations which, moreover, allow an easier optimisation of the various geometrical and physical parameters.

Presented at
Third International Congress on Thermal Stresses
THERMAL STRESSES '99
13-17 June 1999, Cracow, Poland

Geneva, Switzerland,
13 July 1999

Transient quasi-static thermal stresses in a bar subject to transverse 2D-Gaussian heating and to lateral cooling

S. Péraire

European Laboratory for Particle Physics, CERN, CH-1211 Geneva 23, Switzerland.

This paper is divided into three parts. The first part presents the analytical study of the transient thermal field produced in a rectangular bar, by a transverse 2D-Gaussian heating generated from a time dependent trapezoidal function. The bar is laterally cooled, and the two lateral heat transfer coefficients may be different. The thermal diffusivity is assumed to be temperature dependent.

The second part is split into two steps of quasi-static stress analysis. In the first step, a generalised Airy equation of compatibility is solved in the case of elastic plane strain with free uniform longitudinal expansion, while the boundary conditions are left unsatisfied. The second step cancels the remaining spurious stresses at the boundary. Young's modulus and thermal expansion coefficient are assumed to be temperature dependent.

In the last part, numerical aspects are discussed, and results compared with finite element calculations.

Key words**:** *Transient, quasi-static, 2D-Gaussian, bar.*

1 Introduction

Many of the CERN secondary-particle production targets are plate shaped, and intercept a centred 'slow' extracted (order of ms) primary beam, which heats the material. This heat distribution can be modelled as Gaussian profiles in both the horizontal and vertical transverse planes. Modern techniques such as finite element methods provide fast and reliable analyses of the transient thermal and mechanical response of such a 'slow' process (no dynamic effects). However, it is of interest to compare these results with those obtained by simplified analytical calculations which, moreover, allow an easier optimisation of the various geometrical and physical parameters.

The main quantities, symbols and units used in this study are listed in Table 1.

Table 1: Main quantities, symbols and units.

Quantity	Symbol	Unit
Cartesian coordinate	x, y, z	mm
Transverse ½ dimension	l_x, l_y	mm
Gaussian factor	b_x, b_y	mm^{-2}
Biot's number per unit length	h_x, h_y	mm^{-1}
Diffusivity	a	mm^2/s
Temperature rise	T, T_0	°C
T/T_0	T^*	--
Time	t, θ	s
m^{th} root of Eq. (6)	α_{xm}	mm^{-1}
see Eqs (7, 8)	γ_{xm}	--
Lin. thermal expansion coef.	α	10^{-6}/°C
Poisson's ratio	ν	--
Young's modulus	E	GPa
Stress, pressure	σ, τ, p	MPa

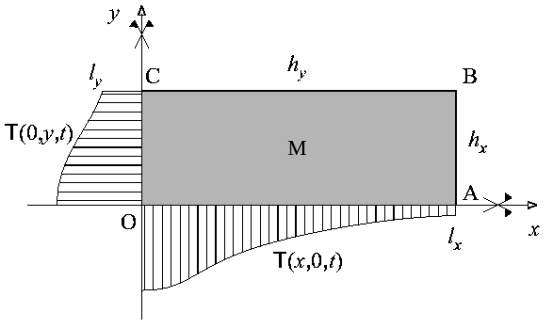

Figure 1: Temperature rise distribution in the ¼ transverse section of the rectangular bar.

2 Transient thermal analysis

An infinite rectangular bar of $2l_x \times 2l_y$ transverse dimensions (see Fig. 1) is subjected to the following heating distribution, T_i :

$$T_i(x,y,t) = T_0 \cdot \exp\left(-b_x \cdot x^2 - b_y \cdot y^2\right) \cdot F(t). \qquad (1)$$

In the interval $(0, 2t_2)$, the dimensionless $F(t)$ function is defined by the speed and duration $(2t_2)$ of the heat load of the bar (see § *2.2.1*). The subsequent transient thermal field $T(x,y,t)$ should satisfy Fourier's equation :

$$\frac{\partial T}{\partial t} = a \cdot \left(\frac{\partial^2 T}{\partial x^2} + \frac{\partial^2 T}{\partial y^2} \right) + \frac{\partial T_i}{\partial t}, \qquad (2)$$

with $$\frac{\partial T}{\partial x}(l_x, y, t) = -h_x \cdot T(l_x, y, t), \qquad (3)$$

and $$\frac{\partial T}{\partial y}(x, l_y, t) = -h_y \cdot T(x, l_y, t). \qquad (4)$$

The Biot's number per unit length h is defined as the ratio of convective heat transfer coefficient to thermal conductivity of the material.

In order to solve this differential equation more easily, a 1D instantaneous (t_2=0) heat load is assumed first; a 2D instantaneous heating is then considered and, finally, the function F(t) is introduced, which generates a progressive heating.

2.1 INSTANTANEOUS HEATING

2.1.1 1D-Gaussian For b_y, h_y =0, the solution of Fourier's equation is [1]:

$$T_x^* = \sum_{m=1}^{\infty} \gamma_{xm} \cdot \cos\alpha_{xm} x \cdot \exp\left(-a\alpha_{xm}^2 t\right), \quad (5)$$

the three infinite series α_x , β_x and γ_x being defined as :

$$\alpha_{xm} \cdot \mathrm{tg}\,\alpha_{xm} l_x = h_x , \quad (6)$$

$$\beta_{xm} = \int_0^{l_x} \exp\left(-b_x x^2\right) \cdot \cos\alpha_{xm} x \,\mathrm{d}x , \quad (7)$$

$$\gamma_{xm} = \frac{2\cdot(h_x^2+\alpha_{xm}^2)}{(h_x^2+\alpha_{xm}^2)\, l_x + h_x} \cdot \beta_{xm} . \quad (8)$$

For b_x, h_x =0, T_y^* is defined in the same way.

2.1.2 2D-Gaussian The solution T_{xy}^* of Eq (2) is now the product $T_x^* \cdot T_y^*$:

$$T_{xy}^* = \sum_{m=1}^{\infty}\sum_{n=1}^{\infty} \Gamma_{mn} \exp -a\left(\alpha_{xm}^2+\alpha_{yn}^2\right)t \ , \quad (9)$$

where

$$\Gamma_{mn}(x,y) = \gamma_{xm} \cdot \gamma_{yn} \cdot \cos\alpha_{xm} x \cdot \cos\alpha_{yn} y . \quad (10)$$

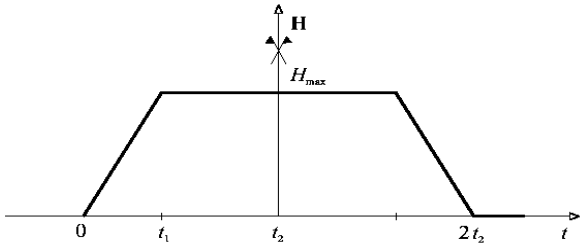

Figure 2: Heat load function.

2.2 PROGRESSIVE HEATING

2.2.1 Heat load The heat load history is described by a symmetric trapezoidal function H(t) of rise and fall time t_1, and of duration $2t_2$ (see Fig. 2). Its maximum value $H_{\max}$ is equal to $1/(2t_2-t_1)$, in order to satisfy :

$$\int_0^{2t_2} \mathrm{H}(\theta)\,\mathrm{d}\theta = \mathrm{F}(2t_2) = 1 . \quad (11)$$

2.2.2 General solution Under this heating condition, the transient thermal field is :

$$T_{xy}^* = \sum_{m=1}^{\infty}\sum_{n=1}^{\infty} \Gamma_{mn} \int_0^t \mathrm{H}(\theta) \exp -a\left(\alpha_{xm}^2+\alpha_{yn}^2\right)(t-\theta)\,\mathrm{d}\theta , \quad (12)$$

which also satisfies the initial condition T(x, y, 0)= 0.

Table 2: Input data, in units defined in Table 1.

Symbol	Value	Symbol	Value
l_x, l_y	10, 1.5	t_1, t_2	10^{-3}, $3\cdot10^{-3}$
b_x, b_y	2, 0.2	$\alpha_{20°}$, $\alpha_{200°}$	12, 14
h_x, h_y	$5\cdot10^{-2}$, 10^{-3}	ν	0.03
$a_{20°}$, $a_{200°}$	44, 25	$E_{20°}$, $E_{200°}$	300, 290
T_0	200		

2.3 NUMERICAL APPLICATION

As a realistic example, a flat high intensity beryllium target is considered here. The input data are listed in Table 2, in units defined in Table 1. T_0, b_x and b_y are derived from particle cascade simulation programs, such as FLUKA [2] . h_y correspond to a forced convective air cooling, and h_x is supposed to roughly account for a partial thermal contact with the aluminium support of the target. E, α and a are assumed to vary linearly from 20°C to 200°C.

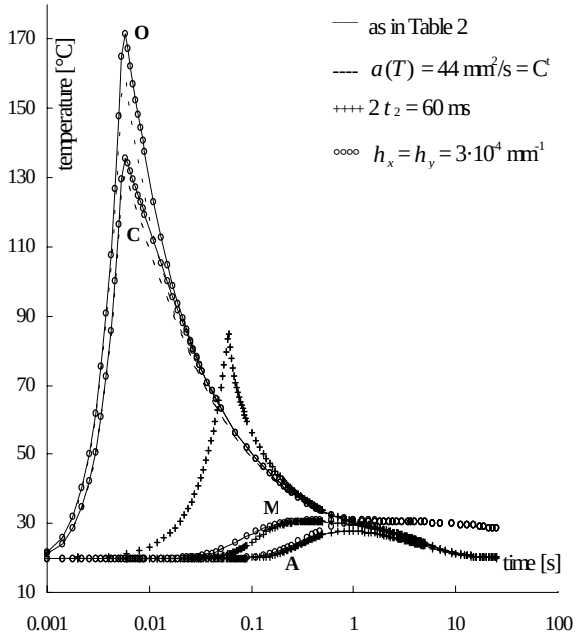

Figure 3: Temperature evolution of points O, A, C and M, under various assumptions.

The temperature evolution of some typical points of the ¼ section is shown in Fig. 3, under various assumptions; those defined in Table 2 are drawn in solid lines. The maximum temperature of 172°C is reached on-axis at the end of heating (t= 6 ms). About 21 s are needed to bring the whole bar to a uniform temperature, *i.e.* to cancel any thermal stress. Note that the dashed curves, which assume a constant thermal diffusivity $a_{20°}$, display an appreciably different temperature level. This level is also strongly affected by the heating duration; a ten times longer heating (60 ms) decreases the maximum temperature by a factor 2 ('crosses' curves). The cooling conditions affect level and time at which the temperatures equalise ('circles' curves); 31°C after 1.7 s for natural air convection (h_x=h_y=$3\cdot10^{-4}$ mm^{-1}).

3 Quasi-static stress analysis

At any moment *t* of the transient process, the second spatial derivatives of the thermal field T^*_{xy} can be calculated from Eq. (12). On this basis, a generalised Airy equation may be used to infer the corresponding stress field σ_x, σ_y, σ_z, τ_{xy}. Elastic plane strain with free longitudinal expansion is assumed: $\varepsilon_z(x,y)=C^t$.

3.1 AIRY EQUATION AND FUNCTIONS

The generalised Airy equation of compatibility is [3] :

$$\frac{\partial^4\varphi}{\partial x^4}+2\frac{\partial^4\varphi}{\partial x^2\partial y^2}+\frac{\partial^4\varphi}{\partial y^4}=\sigma_0\left(\frac{\partial^2 T^*}{\partial x^2}+\frac{\partial^2 T^*}{\partial y^2}\right), \quad (13)$$

$\varphi(x,y)$ being defined (in absence of body load) as :

$$\sigma_x=\frac{\partial^2\varphi}{\partial y^2}, \quad \sigma_y=\frac{\partial^2\varphi}{\partial x^2}, \quad \tau_{xy}=-\frac{\partial^2\varphi}{\partial x\partial y}, \quad (14)$$

and σ_0 being equal to : $\dfrac{-E\alpha T_0}{1-\nu}$.

The problem is then to find Airy functions $\varphi(x,y)$ which also satisfy the boundary conditions :

$$\sigma_x(l_x,y)=\sigma_y(x,l_y)=\tau_{xy}(l_x,y)=\tau_{xy}(x,l_y)=0. \quad (15)$$

3.1.1 Thermal strain compatibility The following 'thermal' Airy function $\varphi_t(x,y)$:

$$\varphi_t=\sigma_0\sum_{m=1}^{\infty}\sum_{n=1}^{\infty}\lambda_{mn}\cos\alpha_{xm}x\cdot\cos\alpha_{yn}y, \quad (16)$$

where $\lambda_{mn}=-\dfrac{\gamma_{xm}\cdot\gamma_{yn}}{\alpha_{xm}^2+\alpha_{yn}^2}$, (17)

satisfies Eq. (13), but not Eqs (15); one writes :

$$\sigma_x(l_x,y)=-p_x(y), \quad \sigma_y(x,l_y)=-p_y(x). \quad (18)$$

It is then required to superimpose two more Airy functions to cancel the spurious external pressures p_x and p_y (the boundary value of τ_{xy} is discussed in § 3.2).

3.1.2 Mechanical strain compatibility The following 'mechanical' Airy function $\varphi_{px}(x,y)$: (19)

$$\varphi_{px}=\sum_{m=1}^{\infty}\left(A_{xm}\omega_{xm}x\cdot\mathrm{sh}\omega_{xm}x+B_{xm}\cdot\mathrm{ch}\omega_{xm}x\right)\cdot\cos\omega_{xm}y$$

where $\omega_{xm}=(m-0.5)\pi/l_y$, (20)

and $A_{xm}=\dfrac{\mathrm{sh}\,\omega_{xm}}{\omega_{xm}^2\left(\omega_{xm}\,l_x+\mathrm{sh}\omega_{xm}\,\mathrm{ch}\omega_{xm}\right)}\cdot C_{xm}$, (21)

$$B_{xm}=-\frac{\mathrm{sh}\omega_{xm}+\omega_{xm}\,l_x\,\mathrm{ch}\omega_{xm}}{\omega_{xm}^2\left(\omega_{xm}\,l_x+\mathrm{sh}\omega_{xm}\,\mathrm{ch}\omega_{xm}\right)}\cdot C_{xm}, \quad (22)$$

satisfies Eq. (13) when making σ_0 = 0, and the two boundary conditions :

$$\sigma_x(l_x,y)=p_x(y)-p_x(l_y), \quad \tau_{xy}(l_x,y)=0. \quad (23)$$

The infinite series C_x is defined as:

$$\sum_{m=1}^{\infty}C_{xm}\cdot\cos\omega_{xm}y=p_x(y)-p_x(l_y). \quad (24)$$

φ_{py} is defined in the same way.

All the functions defined in this chapter are, obviously, also time dependent.

3.2 STRESS FIELDS

Each of the three Airy functions φ_t, φ_{px} and φ_{py} provides a stress field derived from Eqs (14). The complete stress solution results from their superimposition increased by the constant fields $p_x(l_y)$ and $p_y(l_x)$.

Note that the boundary value of τ_{xy} derived from φ_t is not strictly zero. Nevertheless, it is proportional to h_x (in AB) or h_y (in BC), and then practically negligible.

The longitudinal stress σ_z is computed as follows :

$$\sigma_z=\sigma_{z0}-\frac{1}{l_x l_y}\cdot\int_0^{l_y}\int_0^{l_x}\sigma_{z0}\,dx\,dy, \quad (25)$$

where $\sigma_{z0}=\nu(\sigma_x+\sigma_y)-E\alpha T(x,y)$; (26)

σ_{z0} is the value of σ_z if ε_z is assumed to be zero.

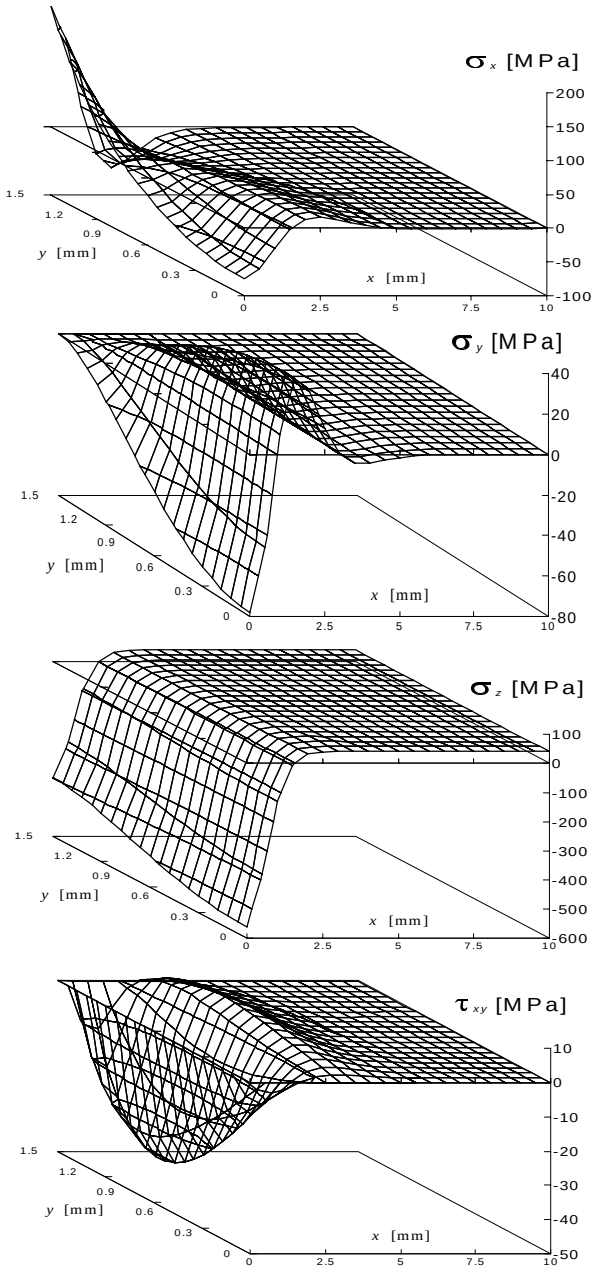

Figure 4: Charts of σ_x, σ_y, σ_z and τ_{xy} fields, at 6 ms.

3D charts of σ_x, σ_y, σ_z and τ_{xy} fields at 6 ms, are displayed in Fig. 4 which shows that, in the ¼ transverse section OABC, σ_x is within –75 and 180 MPa, σ_y within –80 and 40 MPa, σ_z within –560 and 40 MPa, and τ_{xy} within –40 and 10 Mpa; σ_x, σ_y and σ_z are symmetrical about O*x* and O*y* axis, while τ_{xy} is anti-symmetric. The boundary conditions defined by Eq. (15) are satisfied, as well as the symmetry conditions :

$$\frac{\partial \sigma}{\partial x}(0,y)=\frac{\partial \sigma}{\partial y}(x,0)=0\ ,\ \tau_{xy}(0,y)=\tau_{xy}(x,0)=0 \quad (27)$$

The equivalent stress σ_{eq} (Von Mises criterion) is shown in Fig. 5; it reaches 515 MPa at point C. This point is therefore the most critical of the section, though it is not the hottest (135°C). It will probably suffer plastic deformation or even worse local damage, as the yield and ultimate strengths of the beryllium are respectively about 350 MPa and 470 MPa at this temperature. This important aspect is yet out of the scope of the present study.

The longitudinal strain ε_z is uniform over the transverse section, and equal to $1.4 \cdot 10^{-4}$.

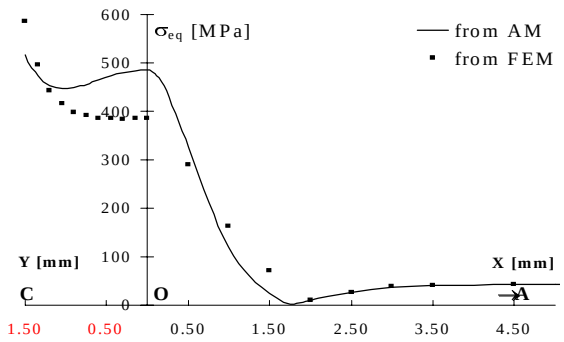

Figure 5: Equivalent stress σ_{eq} (Von Mises criterion) from the two methods, at 6 ms.

4 Numerical aspects

Several stratagems are used to make the computation easier and/or faster :

- *m* and *n* are limited to 80; an absolute convergence criterion (generally 10^{-12}) is furthermore applied to some slow algorithms.
- The first 80 positive roots α of Eq. (6) are computed from:

$$f(\alpha^*) = \alpha^* \cdot \mathrm{tg}\alpha^* - h \cdot l\ , \qquad \alpha^* = \alpha \cdot l\ ; \quad (28)$$

a rough estimation is first obtained by scanning the function by steps of 10^{-2} to detect changes of sign; this is then refined by an iterative minimisation of $|f(\alpha^*)|$ within the step interval.

- In spite of an existing analytical solution, values of β from Eq. (7) are numerically integrated, in order to avoid overflow problems.
- Even though the diffusivity *a* should be a constant in Eq. (2), it is strongly temperature dependent. To overcome this difficulty, *a* is iteratively adapted to the local temperature:

$a_{20°} \rightarrow T_1 \rightarrow a(T_1) \rightarrow T_2 \rightarrow a(T_2)$…up to $|T_n - T_{n-1}| \le 0.1$°C.

- Coefficients *C* of Eq. (24) are time dependent. Nevertheless, they are computed only for several typical times, and then logarithmically interpolated . For a typical time *t* and for each plane *x* and *y*, the 80 coefficients are derived by inverting a 80×80 matrix which accounts for 80 different values of *y* in p_x (or of *x* in p_y).

The computer code was developed in Nodal, an interpretative language similar to Basic and very well suited to iterative processes. Its translation into a more portable language is under consideration.

5 Comparison with the FEM

A plane strain finite element model (FEM) has been analysed by ANSYS [4], in order to check the validity and accuracy of the present analytical method (AM). The same input data were used. The material density ρ was assumed to be constant (1.85 g/cm^3) as well as its specific heat C_p (2 J/g°C); the thermal conductivity λ then varying according to *a* ($\lambda_{20°}$=1.63 W/cm°C, $\lambda_{200°}$= 0.93 W/cm°C) :

$$\lambda = a\ \rho\ C_p\ ; \quad (29)$$

H_{max} (200 s^{-1}) was converted into D_{max} (148 kW/cm^3):

$$D_{max} = T_0\ \rho\ C_p\ H_{max}\ . \quad (30)$$

The ¼ transverse section OABC was meshed into 450 rectangular elements : Δx= 0.08 to 0.33 mm, Δy= 0.1 mm. Figure 5 shows the equivalent stress σ_{eq} obtained by the two methods, at 6 ms along COA. The results are in reasonable agreement, as it is the case for the other components σ_x, σ_y and τ_{xy}, from which σ_{eq} is derived. In spite of local discrepancies, the strong topographical similarity of such complex stress fields validates the AM; its accuracy is similar to that of the FEM.

Acknowledgement

Many thanks to my colleagues Paola Sala-Ferrari and Luca Bruno. Paola, as an eminent FLUKA specialist, performed the necessary heat load modelling. Luca, as an ANSYS expert, checked the analytical results and provided me with fruitful comments and advise.

References

[1] H.S. Carslaw, J.C. Jaeger, “Conduction of Heat in Solids”, Oxford University Press, 1992.

[2] A. Fassò, A. Ferrari, J. Ranft, P.R. Sala, “An update about FLUKA”,CERN TIS-RP/97-05, Genève, 1997.

[3] Muskhelishvili, N.I., “Some basic problems of the mathematical theory of elasticity”, Noordhoff 1953.

[4] “ANSYS Theory Reference - Release 5.4”, Eighth Edition, SAS IP, Inc, September 1997.